ChemComm

COMMUNICATION

View Article Online
View Journal | View Issue

Cite this: *Chem. Commun.*, 2015, 51, 8668

Received 16th March 2015,
Accepted 16th April 2015

DOI: 10.1039/c5cc02222c

www.rsc.org/chemcomm

Microengine-assisted electrochemical measurements at printable sensor strips†

Stefano Cinti,[ab] Gabriela Valdés-Ramírez,[a] Wei Gao,[a] Jinxing Li,[a] Giuseppe Palleschi*[b] and Joseph Wang*[a]

A new microengine-based built-in-platform exploiting a surprising dual action with solution mixing and control of the reaction parameters, has been applied for accelerating chemical reactions (organophosphorous nerve agents hydrolysis) and electrochemical detection of non-hazardous by-product (*p*-nitrophenol) using printable sensor strip.

The growing exploitation of advanced screen-printing fabrication techniques allows for the widespread replacement of conventional ('beaker-type') electrochemical cells and bulky electrodes with easy-to-use sensor strips.[1,2] Such printable sensors permit simple, rapid, centralized and decentralized electrochemical analyses of microliter volumes. Yet, unlike traditional large cells that employ solution stirring or electrode rotation for enhancing the response *via* convective mass transport,[3] microcells based on printable strips are limited to quiescent solutions and hence solely to diffusion transport.

Here, we describe a new concept of microengine-assisted electrochemical measurements using strip-based micro-volume electroanalysis. We demonstrate the dramatic enhanced amperometric signal of organophosphorous (OP) nerve agent detection in the presence of bubble-generating magnesium Janus microengines. The generated microbubbles induce localized convection and a greatly enhanced mass transport and sensitivity.

As recently reported,[4,5] the hydrogen-bubble generation from magnesium-based microengines involves the oxidation of the Mg surface to reduce water:

$$Mg(s) + 2H_2O(aq) \rightarrow Mg(OH)_2(s) + H_2(g).$$

Bubble-propelled microengines have been shown recently to generate a dramatically enhanced fluid transport even when confined into a stationary surface.[6] Such fluid convection from the bubbles generating PANI/Pt tubular microengines has been demonstrated using the displacement of passive microparticle tracers. The fluid transport induced by water-driven Mg micromotors is shown here for a dramatic mixing effect for the electroanalysis of microliter samples at planar strip electrodes. Such unique coupling of microengines and sensor strips is demonstrated toward the amperometric measurements of OP nerve agent degradation.

OP chemical warfare agents and pesticides interrupt the nervous stimuli communication by blocking the enzyme acetylcholinesterase (AChE).[7,8] OP electrochemical detection relies on the enzymatic inhibition of cholinesterase (ChE) or hydrolysis of OP nerve agents by organophosphorous hydrolase (OPH); however these bio-approaches are characterized by long incubation times, enzymes stabilization and enzymes engineering.[9–11]

Recent advances in chemically-powered microscale motors have led to new capabilities and novel applications,[12–14] including new biosensing strategies based on the direct isolation of target or changes in their movement in the presence of target analytes.[15–19] For example the motion of PANI/Pt micromotors has shown to enhance colorimetric immunoassays.[20] Here we exploit for the first time the dual action of water-powered magnesium-based microengines, not only to impart an enhanced fluid mass transport, but also to increase dramatically the pH solution allowing a quick degradation and subsequent detection of OP nerve agents without the need of any external reagents or instruments. These effects are produced by confining the microengines onto the strip surface keeping them without propelling through the sample (Fig. S1, ESI†). The use of bubble-generating Mg Janus microengines is visibly capable to degrade in a short time paraoxon, producing *p*-nitrophenol which is electrochemically detectable. The simple design and operation make this approach a universal route for variety of electrochemical assays of microliter samples at different sensor strips. The new concept simplifies such measurements and can be readily extended to different electrochemical sensing platforms and target analytes, while eliminating the need for additional stimuli, instrument or external stirrer to homogenize ultrasmall samples during their analyses.

[a] *Department of Nanoengineering, University of California San Diego, La Jolla, California 92093-0448, USA. E-mail: josephwang@ucsd.edu*
[b] *Dipartimento di Scienze e Tecnologie Chimiche, University of Rome Tor Vergata, Via della Ricerca Scientifica 1, 00133 Rome, Italy. E-mail: giuseppe.palleschi@uniroma2.it*

† Electronic supplementary information (ESI) available: Additional information pertaining to fabrication procedures, methods and characterization. See DOI: 10.1039/c5cc02222c

As widely stated, regular magnesium microparticles in water produce hydrogen bubbles and magnesium hydroxide; yet hydrogen production is not vigorous since the surface of the Mg microparticles is readily passivated by the formation of hydroxide layer. However, coating Mg microspheres with a gold layer,[4] and the presence of chloride ions allow the reaction to proceed by exploiting the combination of galvanic corrosion and pitting corrosion effects, resulting in a continuous hydrogen bubbles evolution as reported as follows:

$$Mg^{+}(aq) + H_2O(aq) \rightarrow 1/2H_2(g) + Mg^{2+}(aq) + OH^{-}(aq).$$

Here we exploit the generation of both microbubbles and hydroxyl ions with the corresponding increased pH towards degradation enhanced at non-enzymatic strip-based assays of OP nerve agents. Such dual action of micromotors and improved amperometric detection is accomplished with fixed Mg microengines confining them onto the strip surface. The vigorous and prolonged bubble production leads to a greatly enhanced 'built-in mixing' and mass transport effects within the microliter sample droplet, thus allowing a rapid and reproducible nerve-agent degradation with a subsequent detection without the need of external stirrers or mixing devices. The presence of the nickel layer in the Janus microparticles allows the magnetic confinement of the microengines on the sensor strip, preventing their movement to the electrodes area avoiding interference during the electrochemical measurements. An effective fluid transport is achieved in the presence of the generated bubbles, leading to a prolonged coherent flow near their anchor points and dramatically enhancing mass transport in their vicinity. The rising of a vertical bubbles flow is capable to impart effective convective transport to the entire drop (Fig. 1).

Orozco *et al.*,[6] demonstrated how the fluid transport induced by the rising bubbles is larger than that one induced by the freely swimming catalytic micromotors or Janus-microparticles: fixed motors produce a net force on the fluid depending by $1/r$ (r is the distance from source), whereas, not anchored motors exert a weaker convection field that decays quickly, $1/r^2$. We use microengines capable of producing OH^- ions to increase the medium pH and consequently promote the degradation of paraoxon into a readily detectable *p*-nitrophenol. Fig. 2A shows optical images of a 20 mM paraoxon solution (in 0.1 M KCl) on the sensor strip, taken at different times in the absence and presence of microengines. It is clearly visible that in the absence of the Mg microengines the solution remains colorless with the time demonstrating absence of hydrolysis of paraoxon. Meanwhile, in the presence of Mg Janus particles, paraoxon degrades immediately and, after a minute of reaction the solution is almost entirely yellow due to the produced *p*-nitrophenol and the mixing effect which is visible to naked eye; Fig. 2B shows a schematic representation of the electrode before and after the effect of microengine tasks. At time zero t_0 the probe is only in the presence of nerve agents (colorless) while at the end of the process t_i the solution turns yellow, indicating degradation of the starting OP compound to *p*-nitrophenol.

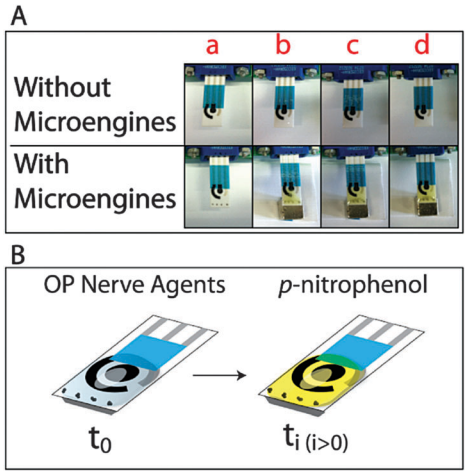

Fig. 2 (A) Time comparison between SPE without and with microengines in the presence of 20 mM paraoxon in 0.1 M KCl after (a) 0, (b) 1, (c) 4 and (d) 10 minutes; (B) Schematic conversion of OP nerve agents to *p*-nitrophenol driven by microengines.

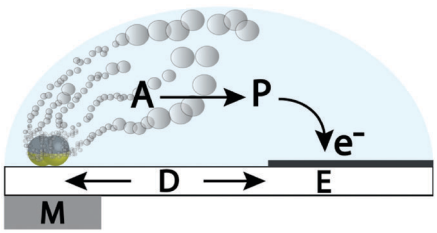

Fig. 1 Microengine-assisted mixing for electrochemical measurements. Schematic illustration of microengine-enhanced bubbles flow. A: OP nerve agents; P: *p*-nitrophenol; E: working electrode; D: distance between working electrode and Mg-microengines (5 mm); M: magnet.

The reactions involved in this Mg Janus/OP nerve agents system are represented in Fig. 3.

Owing to the vigorous production of hydrogen bubbles, the alkaline hydrolyzed by-product, *p*-nitrophenol, is transported throughout the solution allowing the development of a homogeneous solution that is therefore measurable accurately without external stirring. Due to the presence of the magnet located below the strip, the Janus microengines remain confined far from the area of the working electrode. Placing the microengines close to the working electrode area could suppress the electrochemical signal of interest. The microengines were thus positioned as the closest to the electrodes area where their presence does not affect the electrochemical signal.

The electrochemical oxidation of *p*-nitrophenol at carbon electrodes has been widely studied,[21] and we harness the Mg-based Janus microengines for chemical hydrolysis of methyl paraoxon and screen-printed electrodes for the following electrochemical detection of *p*-nitrophenol. Fig. 4 illustrates the cyclic voltammograms related to a 20 mM paraoxon solution. In the absence of Janus particles, no peak is displayed near the 0.9 V (*vs.* Ag/AgCl) whereas in presence of microengines a well-resolved peak is observed at a 0.85 V (*vs.* Ag/AgCl). The oxidation peak position and the intensity of the hydrolyzed paraoxon at 20 mM concentration were compared with *p*-nitrophenol (20 mM) in KCl at

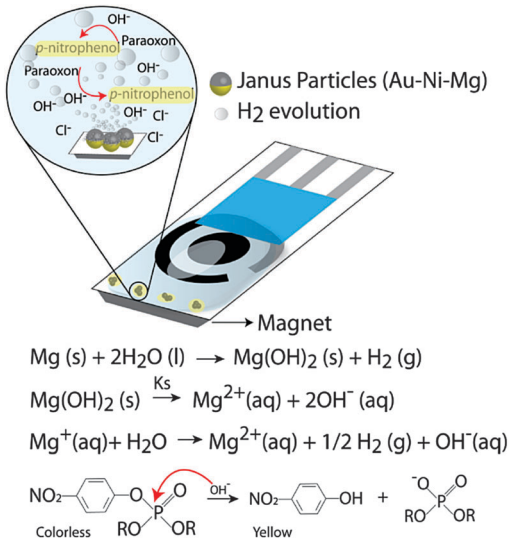

Fig. 3 Mechanism and reactions involved in the OP nerve agents degradation to *p*-nitrophenol accelerated by microengines.

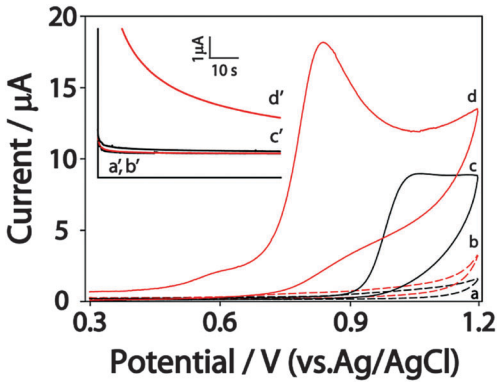

Fig. 4 Cyclic voltammograms of (a) 0.1 M KCl solution without microengines, (b) 0.1 M KCl solution with microengines, (c) 20 mM paraoxon in 0.1 M KCl without microengines and (d) 20 mM paraoxon in 0.1 M KCl with microengines. Inset: amperograms of (a′) 0.1 M KCl solution without microengines, (b′) 0.1 M KCl solution with microengines, (c′) 20 mM paraoxon in 0.1 M KCl without microengines and (d′) 20 mM paraoxon in 0.1 M KCl with microengines.

same pH. The intensity as well as peak position were similar demonstrating not only that after 4 minutes of chemical reaction the paraoxon has been hydrolyzed with a high yield, (Fig. S2, ESI†). The bubbles produced by microengines are capable to produce strong mixing effect generating a homogeneous solution, making attractive the proposed coupled platform. By using similar criteria as for the cyclic voltammetry measurements, amperometric experiments were carried out applying 0.9 V (*vs.* Ag/AgCl) constant potential during 1 min. Inset of Fig. 4 displays that the current responses in the presence of microengines are significantly higher than those obtained using bare SPE. Fig. 5A illustrates the well-defined amperometric response to different nerve agent concentrations up to 20 mM. The corresponding inset displays the corresponding calibration plots and the enhanced sensitivity associated with the presence of the Mg-Janus microengines.

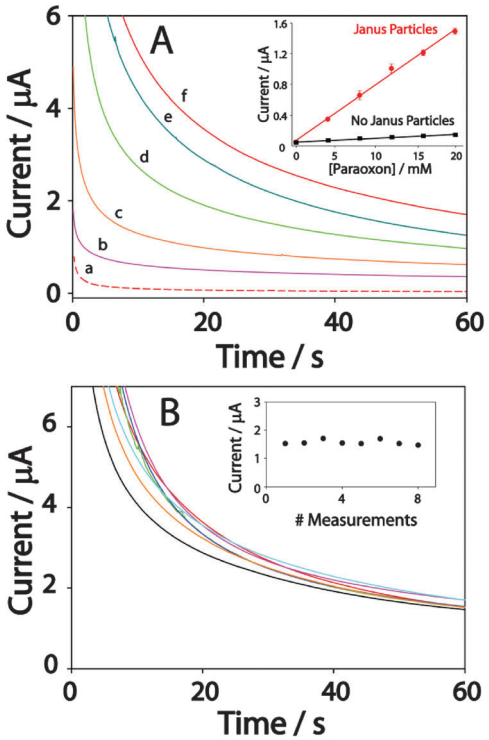

Fig. 5 (A) Amperograms obtained in the presence of microengines for different paraoxon concentrations (a) 0, (b) 4, (c) 8, (d) 12, (e) 16 and (f) 20 mM in 0.1 M KCl. Inset: calibration plot comparison toward paraoxon obtained without (square) and with (circle) microengines, current sampled at 60 s (n = 3); (B) Reproducibility of the response for 20 mM paraoxon solution in KCl 0.1 M in presence of microengines (n = 8). Applied potential, 0.9 V (*vs.* Ag/AgCl).

Linear correlation between current response *vs.* paraoxon concentrations was found as is shown in the inset calibration plot Fig. 5A (correlation coefficient of 0.995). The sensitivity observed in the presence of Janus microengines is significantly larger (~15 fold) compared to electrodes without microengines. Eight different microengines-modified SPEs were used for precision evaluation of the assay: as illustrated in Fig. 5B, these series of measurement at 20 mM paraoxon yielded a reproducible response (RSD < 5%) indicating high reproducibility for the microengine-induced high performing mixing process towards paraoxon degradation and subsequent detection.

In conclusion, we have demonstrated the use of bubble-generating microengines for generating a greatly enhanced fluid transport during amperometric measurements at common printable sensor strips. The presence of magnesium Janus microengines along with OPH makes possible the rapid selective conversion of a non-detectable species (paraoxon) to an electroactive compound (*p*-nitrophenol) easily detectable with an electrochemical strip platform. Such operation addresses the challenge of imparting effective convective transport using microliter volumes strip-based measurements. The microengines operation leads to increase the pH of the solution and a built-in stirring increasing sensitivity towards paraoxon detection, up to 15-fold, compared to a non-engineered bare screen-printed electrode. The magnetically-anchored microengines can serve as an 'artificial' enzyme toward

the hydrolysis (degradation) of OP compounds. The production of an electroactive non-hazardous compound as *p*-nitrophenol was easily detected by a disposable, cost effective and mass-producible screen-printed carbon electrodes. The integration of microengines within an electrochemical strip platform represents an attractive approach for built-in mixing that can be extended to the enhancement of measurements using diverse thick-film and thin-film planar sensor strips for a wide range of practical applications. For example, microengines based on different materials (*e.g.*, Zn, Al, or Pt) can produce microbubbles and mixing in acidic, alkaline or H_2O_2 solutions, and used for the electrochemical measurements in different environments.[22] These bubble-generating microspheres can be combined with different electrode materials for imparting the necessary detection sensitivity and selectivity towards specific analytes.

Defense Threat Reduction Agency-Joint Science and Technology Office for Chemical and Biological Defense (Grant No. HDTRA1-13-1-0002 and HDTRA1-14-1-0064) supported this project. S.C. was economically supported by a PhD fellowship from the Italian Ministry of University and Research (MIUR).

Notes and references

1 J. Wang, *Analyst*, 1994, **119**, 763–766.
2 M. Albareda-Sirvent, A. Merkoçi and S. Alegret, *Sens. Actuators, B*, 2000, **9**, 153–163.
3 J. Wang, *Analytical Electrochemistry*, Wiley-VCH, New Jersey, 3rd edn, 2006.
4 W. Gao, X. Feng, A. Pei, Y. Gu, J. Li and J. Wang, *Nanoscale*, 2013, **4**, 4696–4700.
5 F. Mou, C. Chen, Q. Zhong, Y. Yin, H. R. Ma and J. Guan, *ACS Appl. Mater. Interfaces*, 2014, **6**, 9897–9903.
6 J. Orozco, B. Jurado-Sánchez, G. Wagner, W. Gao, R. Vazquez-Duhalt, S. Sattayasamitsathit, M. Galarnyk, A. Cortés, D. Saintillan and J. Wang, *Langmuir*, 2014, **30**, 5082–5087.
7 C. Albaret, S. Lacoutiere, W. P. Ashman, D. Froment and P. L. Fortier, *Proteins: Struct., Funct., Genet.*, 1997, **28**, 543–555.
8 J. H. McDonough and T.-M. Shih, *Neurosci. Biobehav. Rev.*, 1997, **21**, 559–579.
9 G. Farnoosh and A. M. Latifi, *J. Appl. Biotechnol. Rep.*, 2014, **1**, 1–10.
10 A. Mulchandani, W. Chen, P. Mulchandani, J. Wang and K. R. Rogers, *Biosens. Bioelectron.*, 2001, **16**, 225–230.
11 D. Du, W. Chen, W. Zhang, D. Liu, H. Li and Y. Lin, *Biosens. Bioelectron.*, 2010, **25**, 1370–1375.
12 J. Wang, *Nanomachines: Fundamentals and Applications*, Wiley-VCH, Germany, 1st edn, 2013.
13 W. Wang, W. Duan, S. Ahmed, T. E. Mallouk and A. Sen, *Nano Today*, 2013, **8**, 531–554.
14 M. Guix, C. C. Mayorga-Martinez and A. Merkoçi, *Chem. Rev.*, 2014, **114**, 6285–6322.
15 W. Gao and J. Wang, *ACS Nano*, 2014, **8**, 3170–3180.
16 J. Orozco, V. Garcia-Gradilla, M. D'Agostino, W. Gao, A. Cortés and J. Wang, *ACS Nano*, 2013, **7**, 818–824.
17 D. Kagan, P. Calvo-Marzal, S. Balasubramanian, S. Sattayasamitsathit, K. M. Manesh, G. U. Flechsig and J. Wang, *J. Am. Chem. Soc.*, 2009, **131**, 12082–12083.
18 J. Wu, S. Balasubramanian, S. Kagan, K. M. Manesh, S. Campuzano and J. Wang, *Nat. Commun.*, 2010, **1**, 1–6.
19 J. Wang, *Lab Chip*, 2012, **12**, 1944–1950.
20 E. Morales-Narváez, M. Guix, M. Medina-Sánchez, C. C. Mayorga-Martinez and A. Merkoçi, *Small*, 2014, **10**, 2542–2548.
21 R. P. Deo, J. Wang, I. Block, A. Muclhandani, K. A. Joshi, M. Trojanowicz, F. Scholz, W. Chen and Y. Lin, *Anal. Chim. Acta*, 2005, **530**, 185–189.
22 (*a*) W. Gao, M. D'Agostino, V. Garcia-Gradilla, J. Orozco and J. Wang, *Small*, 2013, **9**, 467–471; (*b*) W. Gao, R. Dong, S. Thamphiwatana, J. Li, W. Gao, L. Zhang and J. Wang, *ACS Nano*, 2015, **9**, 117–123; (*c*) W. Gao, S. Sattayasamitsathit, A. Uygun, A. Pei, A. Ponedal and J. Wang, *Nanoscale*, 2012, **4**, 2447–2453.